Microsyst Technol (2012) 18:581–589
DOI 10.1007/s00542-012-1481-5

TECHNICAL PAPER

Manufacturing and replication of glass pyramidal micro-structures by using the injection moulding process

M. Sahli · C. Millot · J.-C Gelin · T. Barrière

Received: 24 July 2011 / Accepted: 8 March 2012 / Published online: 30 March 2012

Abstract The aim of this work is to perform experimental investigations related to the different injection moulding conditions required for the proper replication of glass structures. The paper investigates the thermal and rheological characterisations of the feedstock. This study demonstrates that the structured shapes could be successfully injected in the structured metallic mould with pyramidal shapes, with suitable forming parameters. After sintering, the experiment results confirm that the components exhibit anisotropic shrinkage in range from 10 to 20 %.

1 Introduction

Powder injection moulding (PIM) is an established mass production process for manufacturing small parts, with accurate complex shaped components from metal and ceramic powders (Cansell and Aymonier 2009; Wiest et al. 2009; Meng et al. 2011a, b). PIM combines the merits of plastic injection moulding as well as powder metallurgy processes, such as suitability for mass production, part shape complexity, low cost and applicability to a large variety of materials. The four typical steps for the MIM process are mixing, injection moulding, debinding and sintering. Initially, a binder with a suitable formulation is mixed with the glass powders to form a feedstock. The binder must provide low viscosity for easy filling of the micro-cavities during injection moulding, high green strength for demoulding, as well as good shape retention and low shrinkage during debinding and sintering (Merz et al. 2002; Gulsoy and German 2008). During moulding the polymer-glass feedstock is injected to get polymeric/glass parts with required shapes. The moulded parts are then submitted a debinding step where the binder is removed. After debinding, the parts are subjected to a sintering step and final products with required properties are obtained as illustrated in Fig. 1 (Boccaccini and Olevsky 1999; Meng et al. 2011a, b).

In recent years, there is a growing interest for glass micro-parts or glass micro-structured components in various application fields offering opportunities such as medical technologies, micro-fluidics, and micro-mechanics (Tay et al. 2005; Pirhonen et al. 2006; Petzoldt 2008). The glass exhibits excellent physical and chemical functions, it is one of the most attractive advanced materials, and many researchers performed a large diversity of research works (Ran 2001; Yong-Taeg et al. 2002).

Czarwinski (1968) considered the process of sintering of glass as an heat treatment that results in the grains adhesion. He considers that that during the first stage of sintering, glass powder transforms into a low-strength porous material. During the second stage, the density can increase up to the monolithic glass one. Boccaccini and Olevsky (1999) studied the isothermal sintering of glass powder compacts containing Al_2O_3 platelet inclusions. It is demonstrated that rigid inclusions influence both the initial and the current states of the porous compact, decreasing anisotropy at the stage of compaction and increasing its current value during sintering. Kingeri and Berg (1955) found that the initial sintering rate of glass powders is directly proportional to the surface tension and inversely proportional to the particle size and the viscosity of glass.

The aim of this work is first to perform experimental research on mixing of various conditions glass powders, injection moulding, debinding and densification adapted to

M. Sahli (✉) · C. Millot · J.-CGelin · T. Barrière
Applied Mechanics Department, CNRS UMR 6174,
ENSMM, Femto-ST Institute, 25030 Besançon Cedex, France
e-mail: Mohamed.sahli@ens2m.fr

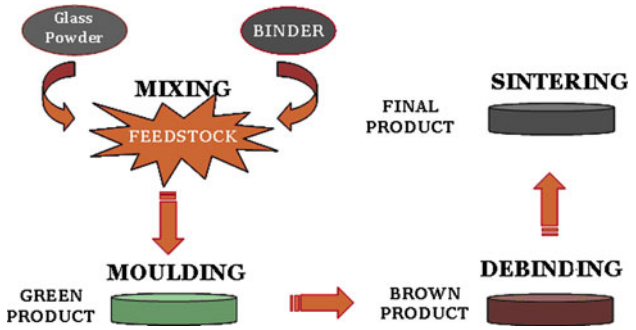

Fig. 1 Schematic manufacturing diagram of glass components by glass powder injection moulding

PIM. This analysis is necessary for proper components replication taking into account the final shrinkage, loss of weight and the effect of temperature on the microstructure of densification. The results finally enable the manufacturing of components of predetermined shapes and geometric dimensions, physical and mechanical properties required from glass with particle size and comparison well mastered.

2 Materials and methods

2.1 Materials

The glass powder particles used in this work was supplied by Sovitec® Company with a density equal to 2.5 g/cm^3. Figure 2 shows the morphology of the glass powder particles obtained by scanning electron microscope (SEM). The average particle size is about 21 μm and specific surface area is equal to 0.861 m^2/g. Particle size distribution is shown in Fig. 3. The glass powders exhibits regular shape particles with particles mostly spherical. The chemical composition of the glass powders is related in Fig. 4.

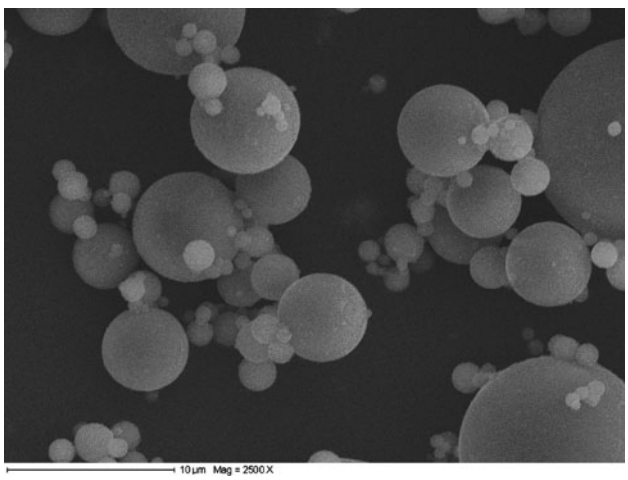

Fig. 2 SEM micrograph of glass powders

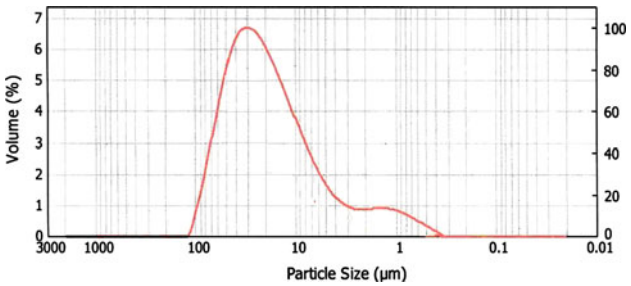

Fig. 3 Particle size distribution of the glass powder (d_{10} = 3 μm, d_{50} = 21 μm, d_{90} = 56 μm)

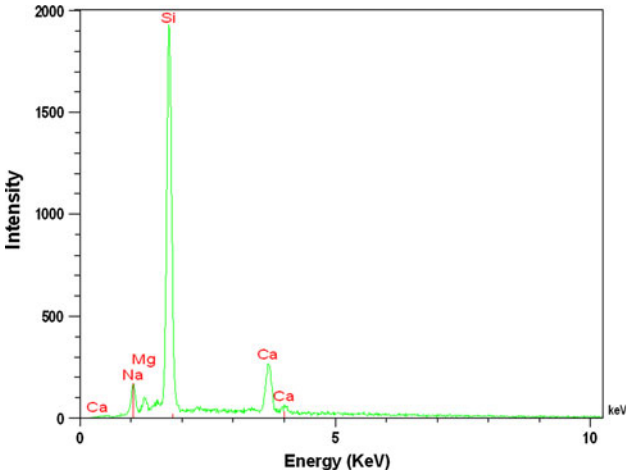

Fig. 4 The plot of intensity versus energy dispersive

A multi-component binder, consisting of the following was used. The binder consists in low density polyethylene (LDPE, Goodfellow®), polypropylene (PP, SA Sigma-Aldrich®), polypropylene (PP, Goodfellow®), paraffin wax (PW, VWR Prolabo®) and stearic acid (SA, Sigma-Aldrich®). Thermal characterizations of the binder components were conducted to facilitate a selection of suitable mixing conditions. Table 1 relates the thermal characteristics of the binder components. The highest melting temperature of the binder components measured on a differential scanning calorimeter (DSC) is 160 °C for PP. The lowest start degradation temperature of the binder measured on a Setaram thermogravimetric analyser (TGA) is 180 °C for SA.

2.2 Preparation of feedstocks

Mixing of the glass powder with the binder was carried out in Brabender® mixer in order to prepare the different feedstocks (see Table 2). The mixing was studied with 5 vol% incremental powder loading, from 35 to 70 vol%. Based on the thermal characterisations of the binder components, the mixing temperature was set at 170 °C, above

Table 1 Characterisation of the three different binder systems used for glass feedstock formulations

Binders	Density	Melting temperature (°C)	Degradation temperature range (°C)
Stearic acid (SA)	0.89	70	160–300
Paraffin wax (PW)	0.91	60	190–340
Polypropylene (PP)	0.90	160	410–520
Low density polyethylene (LDPE)	0.923	120	390–500

Table 2 Characteristic of the polymer/glass feedstock formulations proposed

Formulation	Binders, volume
Feedstock 1	PP(Aldrich®) + PW + SA
Feedstock 2	LDPE(Goodfellow®) + PW + SA
Feedstock 3	PP(Goodfellow®) + PW + SA

the highest melting temperature of 160 °C and below the lowest start degradation temperature of 180 °C. This would facilitate complete melting and prevent binder degradation. Afterwards, the glass powders have been added to the binder by using a sequence of increasing loading stages to achieve the homogenous mixtures. The mixing time was about 120 min. Then the feedstocks are granulated into small pellets for rheology measurements and replications by using injection moulding process. Figure 5 relates to the SEM photo of the glass powder particles that are uniformly distributed in the binder.

The thermal degradation of the feedstock was evaluated by a Setaram® thermogravimetric analyser (TGA), in the range from 25 to 500 °C. The characterizations of the shear viscosity have been performed using a capillary rheometer provided by Bohlin Instruments®. Than the feedstocks were extruded through an axisymmetric die made in tungsten car-bide, with flat bottom, using a ratio length (L) to diameter (D) equal to 16 and an entrance angle equal 180°. All the experiments were performed at 220 °C for the injection temperature and 1 and $10^4 s^{-1}$ for the shear rate.

2.3 Injection moulding

The granulated glass feedstocks were injected using an Arburg® injection moulding press characterised by a maximum injection volume of 12 cm^3. A structured metal die mould was proposed in our laboratory by using EDM. The mould cavities are composed of a series of square pyramids with equal size corresponding to 3 × 3 mm and a height equal to 0.8 mm (Fig. 6). The set of suitable injection moulding parameters used is shown in Table 3.

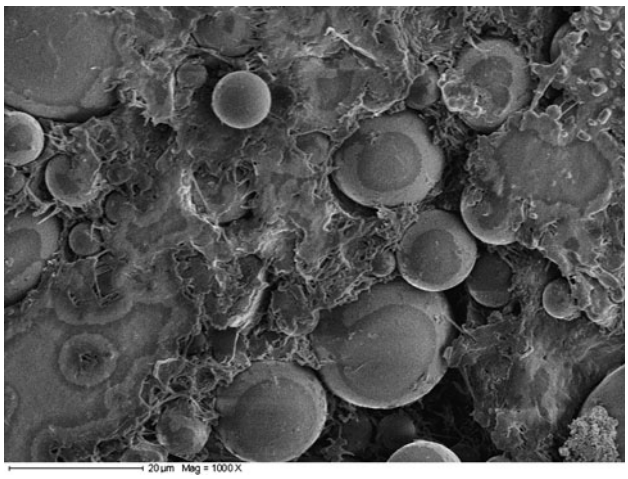

Fig. 5 SEM photo of glass feedstock after mixing (powder volume loading equal 60 %)

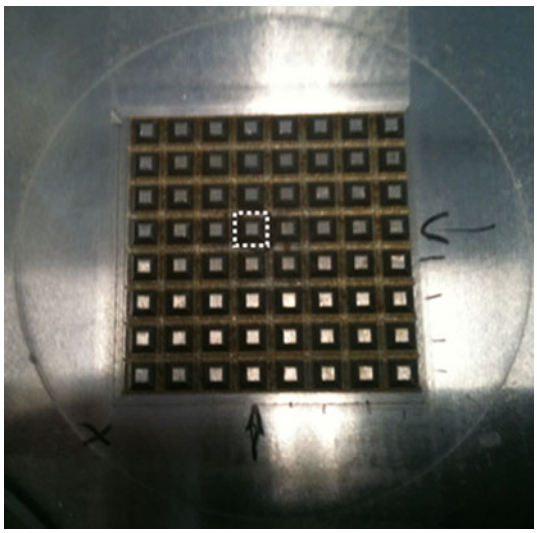

Fig. 6 Geometry of the patterns of metallic mould inserts

Table 3 Suitable injection moulding parameters for the pyramidal part

Moulding parameters	Value
Injection speed (ccm/s)	40
Injection pressure (MPa)	80
Melting temperature (°C)	200
Mould temperature (°C)	25

2.4 Debinding and sintering

The pre-debinding was carried out in two stages, namely the solvent and thermal debinding under argon atmosphere to eliminate some of the binders. The green specimens obtained by injection moulding were immersed in hexane at room temperature for 48 h. Then, under the influence of

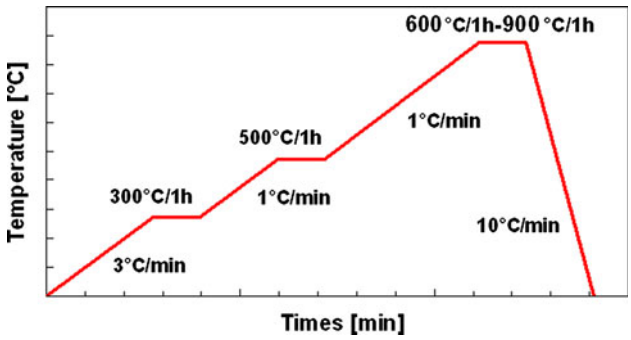

Fig. 7 Thermal debinding and sintering cycle

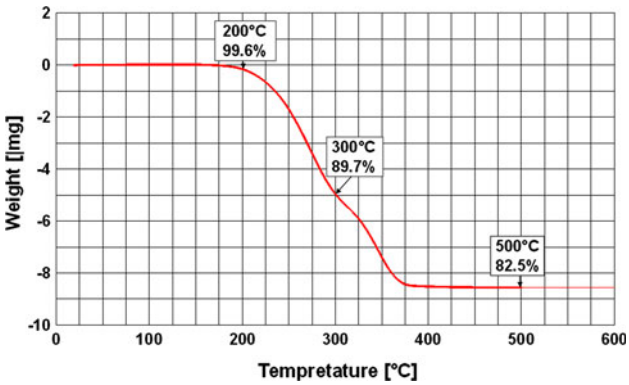

Fig. 8 TGA curve of the feedstock with 60 wt% glass powders

heat, a portion of binder is eliminated during a debinding performed in a thermal oven heated at a temperature equal to 190 °C for 24 h. This step removes the polymeric binders and it result a porous part (called part brown). To consolidate the debinded parts, the samples undergo a heat treatment for densification by solid state diffusion under vacuum in a Vas furnace or under air in a Naber-therm® furnace. The samples were placed in the oven and the temperature was gradually increased by 3 °C/min to 300 °C followed by a second rise at 1 °C/min up to 500 °C. The highest debinding temperature was set to 500 °C to ensure that all the binder components are removed and to facilitate handling. After debinding, densification was achieved for five different sintering temperatures with an heating rate equal to 1 °C/min. This very slow increase in temperature contributes to prevent cracking of the components when the binders start to decompose (Fig. 7). The thermal debinding and sintering stages were conducted according to a suitable temperature profile versus time.

3 Results and discussions

3.1 Thermal properties

Figure 8 shows TG curves of stearic acid, paraffin wax, polypropylene and feedstock. An TG curves, the stearic acid, paraffin wax and polypropylene start to decompose, at above 170, 210 and 300 °C, respectively. The TGA curve indicates two degradation stages. By comparison of the TGA curves, it was reasonable that the full degradation of PW and SA occurred in the first degradation temperature range (170–310 °C), whereas the degradation of PP occurs at higher temperatures (300–410 °C). Above 420 °C, all the binder components were completely burned off. Consequently, the appropriate melting temperature range for injection molding is within in range from 150 to 280 °C.

3.2 Preparation and characterization of glass feedstock

It is necessary to determine an appropriate formulation associated to the fact that efficiency of the feedstocks significantly change due to the physical properties of the binder. Three different mixtures related to the proposed formulations have been tested using a twin screw mixer, according to the same processing conditions. Table 2 gives the binder system details according to the three different proposed formulations. The experimental results that are related in Fig. 9, reveals the mixing behaviour of the glass feedstock ($d_{50} = 20$ μm) with volumetric powder loading equal 60 % denoted as F1, F2 and F3, respectively (see Table 2). The final mixing torque corresponding to formulation 1 is about 4.3 N m compared with 6.8 and 7.1 N m corresponding to formulations 2 and 3.

The mixing tests can be also used for determining the maximum powder loading, by a continuously and gradually increasing powder loading from 35 to 75 % by adding the powders with an increment equals 5 % for each level. The mixing torque versus mixing time is related Fig. 10. Three different zones appear in curve Fig. 10. In zone I, there is mainly binder in the mixture and the torque remains almost at the same low levels (35–55 %). In zone II (55–65 %) the

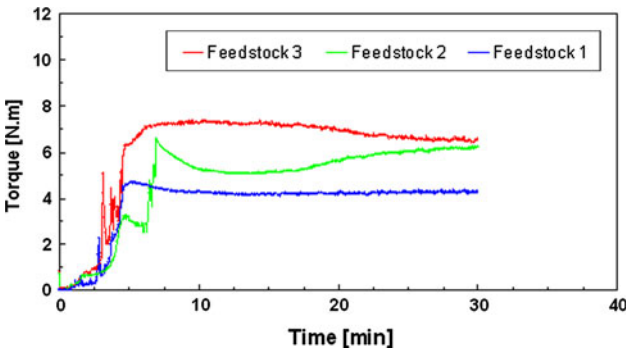

Fig. 9 Mixing torque versus time corresponding to three different feedstocks obtained from the mixing test

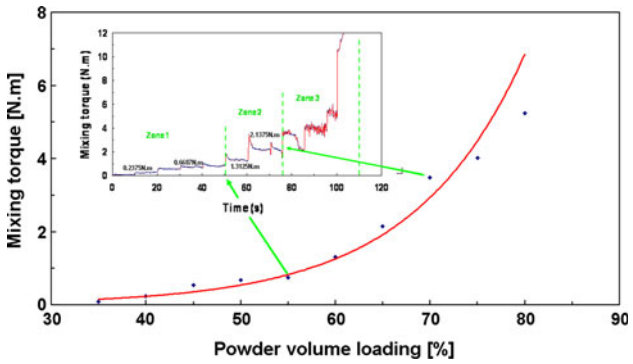

Fig. 10 Mixing torque versus powder volume loading obtained through the continuously rising powder loading technique

torque starts to gradually increase with a better homogenisation. The critical solid volume loading has been determined beyond 70 % (zone III).

Several feedstocks have been prepared using different glass powders corresponding to formulation 1 (Table 2) with different loading ratios. The mixing torques have been measured and plotted versus time in Fig. 11. The picks that appear on the graphs are due to addition of small amounts of powder in the mixture. The final mixing torque is about 2.2 Nm corresponding to 60 vol% powder loading compared to 3.1 and 3.6 Nm for the 65 and 70 vol% powder loading. So one can conclude that 60 % of metal powder loading in volume gives the lowest torque, finally these feedstocks have been retained for the subsequent experiments.

3.3 Rheological properties

The rheological properties of the different feedstocks have been sequentially tested using a capillary rheometer, considering different shear rates with the same capillary die diameter (Ø = 1 mm). Figure 12 relates shear viscosity versus shear rate that corresponds to the rheological characteristics of the feedstocks mixed under the different conditions. The viscosity values of mixtures resulting from

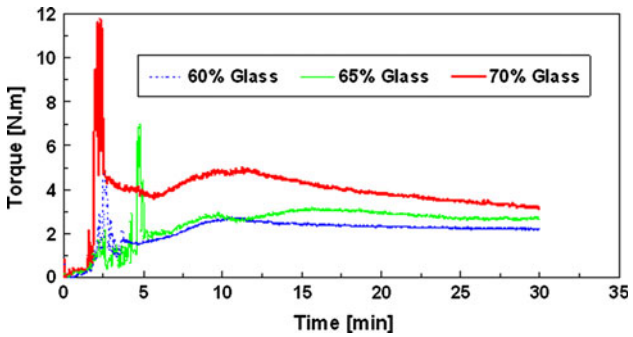

Fig. 11 Mixing torque versus time for three different glass powders loading corresponding to feedstock 1

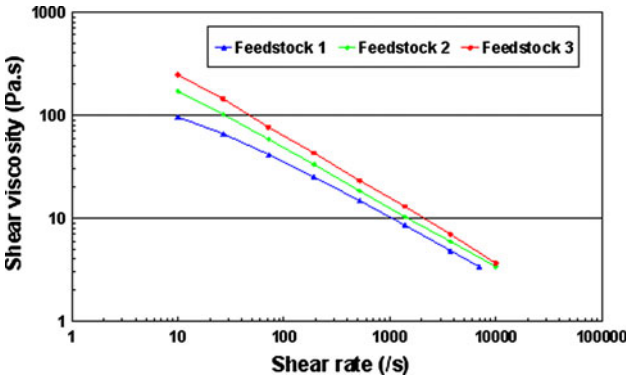

Fig. 12 Shear viscosity versus shear rate measured with a capillary rheometer for two feedstocks measured at 220 °C

formulation 1 are lower than the mixture made with the other two formulations. This trend is the same as that observed when measuring the mixing torque. This confirms that there is a relationship between the pair of mixing and shear viscosity. Based on the results obtained through rheology and mixing tests (Figs. 9, 12), the original formulation used is the first formulation.

Shear viscosity measurements were also performed feedstocks mixtures (F1) at different loading rates with a two-channel capillary rheometer (Fig. 13). It was found that the shear viscosity decreases when the loading rate decreases, which allows it to conclude that a lower loading rate will allow better filling of the mould cavities. It can be observed also that lower viscosities are obtained for the low loading rates (60 % in glass powder loading). So in conclusion, formulation 1 that leads the lowest torque and stabilises faster than the two other one. So this formulation has been retained for the subsequent tests.

3.4 Dimensional change and shrinkage

One can plot the shape the 2D profiles extracted from the imprints replicas and die cavity mould as illustrated in

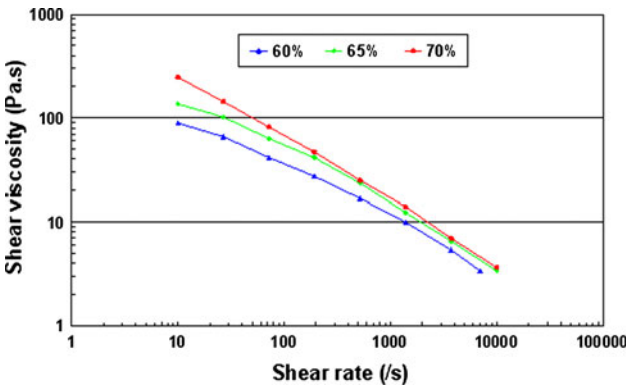

Fig. 13 Shear viscosity versus shear rate measured with a capillary rheometer at different loading rates (capillary die diameter equal 1 mm as the same glass feedstock 1 measured at 220 °C)

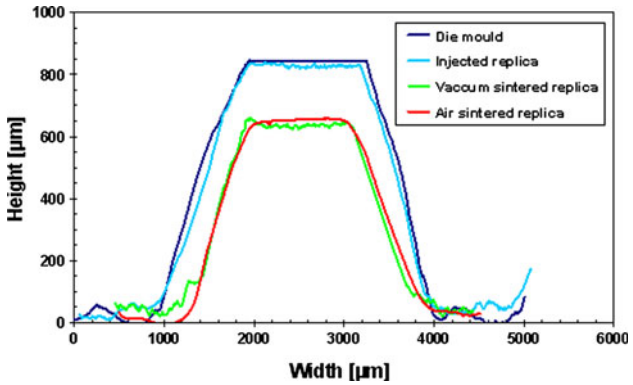

Fig. 14 Comparative variations of 2D topographical profiles of the replicas after injection and sintering of the glass feedstock along the *x*–*x* direction

Fig. 14. From the measurements of all experimental tests, one concludes that the improvement in replication quality is linked to the increase of the temperature during the forming process. After several tests, one found that the temperature strongly influences the resulting filling rates, as well as the final surface roughness of cavities, are can notice that pressure effects are less sensitive. This could be due to the binder fluidity that affects the flows of the feedstock in the different parts of the mould cavity. The corresponding conditions to obtain the replicas are accurately validated for temperature and pressure corresponding respectively to 220 °C and 80 MPa. As example, Fig. 15 relates a comparative 3D cartography to assess proper pyramidal shape replica with appropriate die mould cavity. Figure 16 relates the photograph of the glass parts after undergoing different processing steps.

During thermal debinding and sintering, binder elimination and subsequent particles bonding take place, resulting in dimensional change for the PIM parts. The diameter and thickness of the injected parts are 56 and 3 mm, respectively. The debinded parts are homothetic to the moulded ones, but a small shrinkage around 3 % and mass loss around 5 % is observed (Fig. 17). The sintered parts are carefully measured in order to determine the weight and shrinkage. After the sintering stage, the component undergoes an important anisotropic shrinkage in the range from 8 to 10 % in the radial direction and from 15 at 20 % depending in the thickness direction, depending on the heating rates used in the thermal cycles during sintering (Figs. 14, 16). Moreover, a total mass loss around 20 % is measured. This dimensional change could be compensated when design the mould cavity.

3.5 Density and roughness

Roughness measurements were conducted on components sintered at different temperatures. These values were compared with measurements values realised on the metal mould. It is observed that increasing the sintering temperature causes a slight increase in surface roughness of the parts that is accompanied by a slightly rounding of the ends and corners.

Figure 18 shows the variation of the density measured by hydrostatic weighing, according to the sintering temperature. The hydrostatic density determined by the ratio between the mass of the component in air and its mass in a fluid (pure ethanol). It shows that the sintered density increased from 2.1 to 2.47 g/cm^3 when the sintering temperature increased from 600 to 875 °C. Density at 875 °C is almost equal to 97 % of theoretical density. These results are reinforced by using SEM observations made on samples sintered at different temperatures. SEM pictures taken from the same sections of samples sintered in air at different temperatures are related in Fig. 20. Glass powder structures are clearly revealed in the pictures. Considering Fig. 20, one can easy to distinguish the spherical balls due to the incomplete sintering of the sample, due to the fact that the sintering temperature chosen is too low (Fig. 19).

The micrographs of polished cross-sections of glass replicas have been also illustrated to show the microstructure variation during vacuum sintering or air sintering

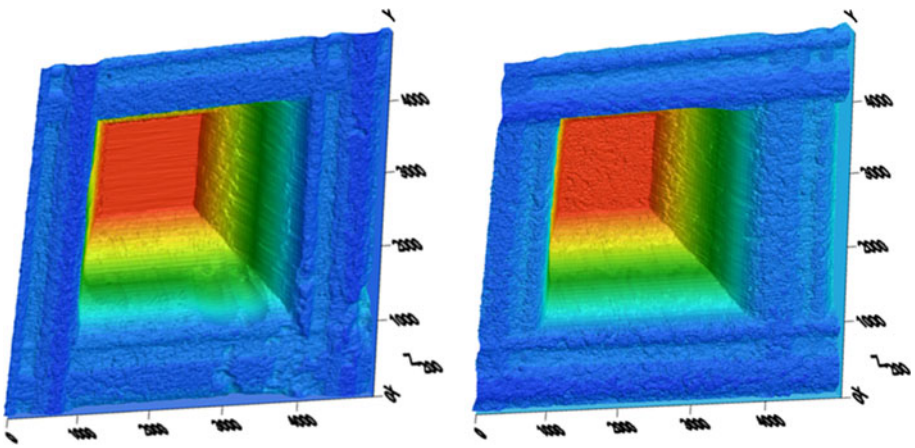

Fig. 15 3D topographies of *pyramidal shape* injected replica compared to die mould cavity at 220 °C

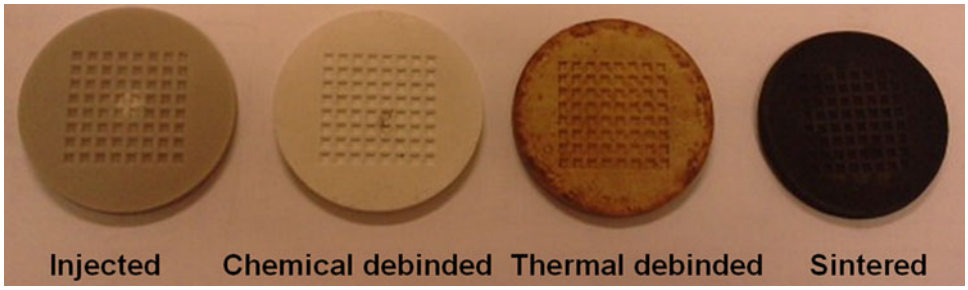

Fig. 16 Photograph of injected, debinded and vacuum sintered glass components

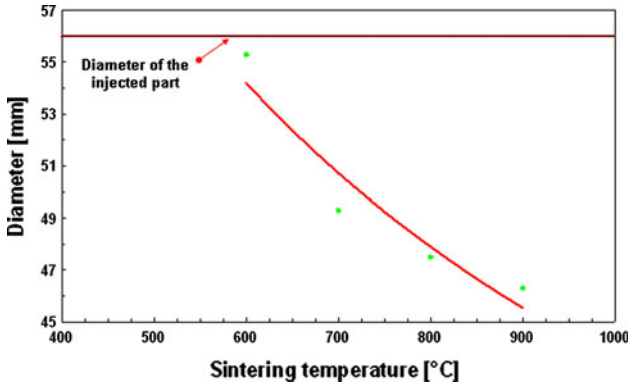

Fig. 17 Diameter of circular parts after different processing steps

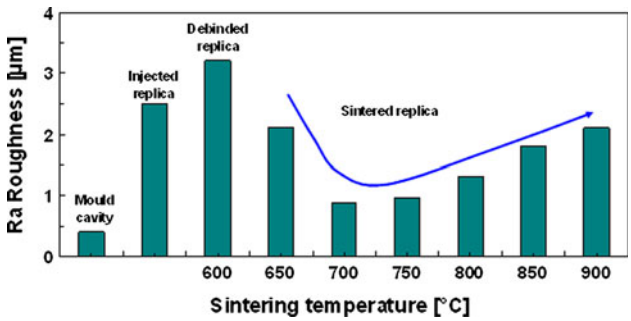

Fig. 18 Roughness evolution of glass parts sintered at different temperatures

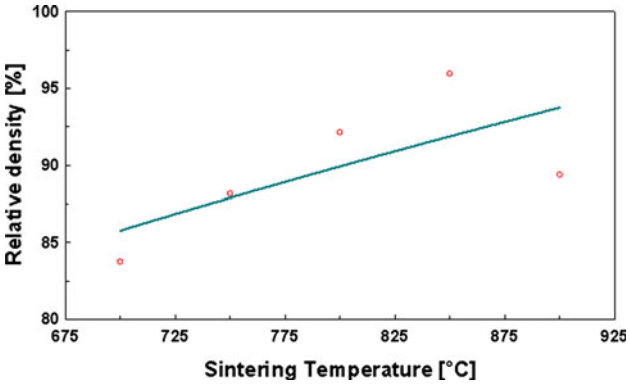

Fig. 19 Sintered densities of glass parts sintered at different temperatures

(Fig. 21). The observations through SEM are carried out on slices of the sintered samples sectioned transversely. One can observe the macro-porous structure formed by glass microspheres and the interconnections between each pore. However, the temperature values between 500 and 600 °C show that the macro-porous structure is not sufficiently sintered in both cases. In addition, the temperature at which it would be interesting to perform the sintering in air is the range from 700 to 850 °C. This temperature range provides a maximum shrinkage, that it results a maximum densification.

Figure 22 shows the photographs of the sintered parts at 700 °C in different conditions (vacuum or air). For vacuum sintering, some pores are visible, occurring between the glass grains at sintering temperature equal to 700 °C (see Figs. 21a, 22a). There is an indication of imperfect and incomplete sintering. Figure 22b is a photograph of the typical sintered parts with proper shape retention without warpage and crack that was achieved nevertheless the corners is slightly rounded.

4 Conclusions

The proposed paper investigates the possibilities to get glass structured parts by injection moulding process. In a first stage, the paper relates and investigates the thermal and rheological characterisations of the feedstock with different combinations of powders and binder systems that enable suitable processing conditions for the moulding and debinding of the glass parts. For the glass powder and binder components used, a powder loading of 60 vol% was established based on steady-state mixing torque. Generally, the viscosity of feedstock is reduced with increasing shear rate, indicated a pseudo-plastic flow behaviour.

In a second stage, and by using the injection moulding process, an experimental investigation performed with three different feedstocks including the different powders. The study on the injection moulding of structured glass replicas demonstrates that the micro-structured shapes could be successfully injected with suitable forming

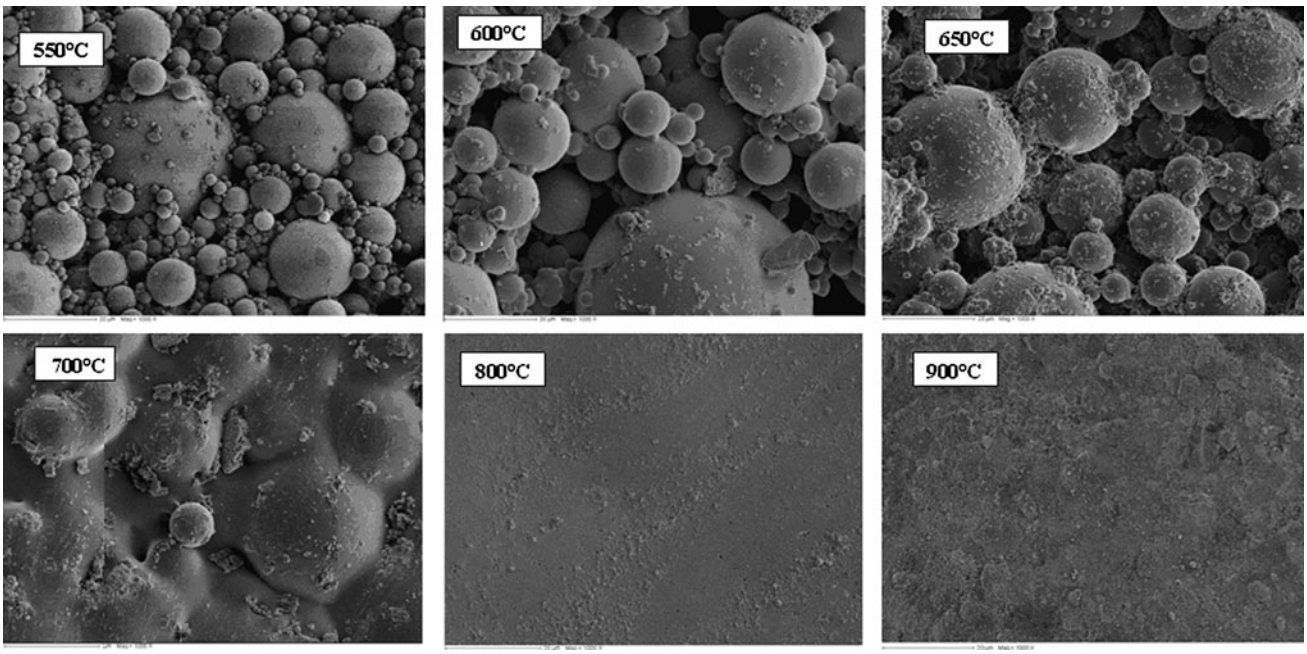

Fig. 20 SEM micrographs of the glass samples sintered at different sintering temperatures

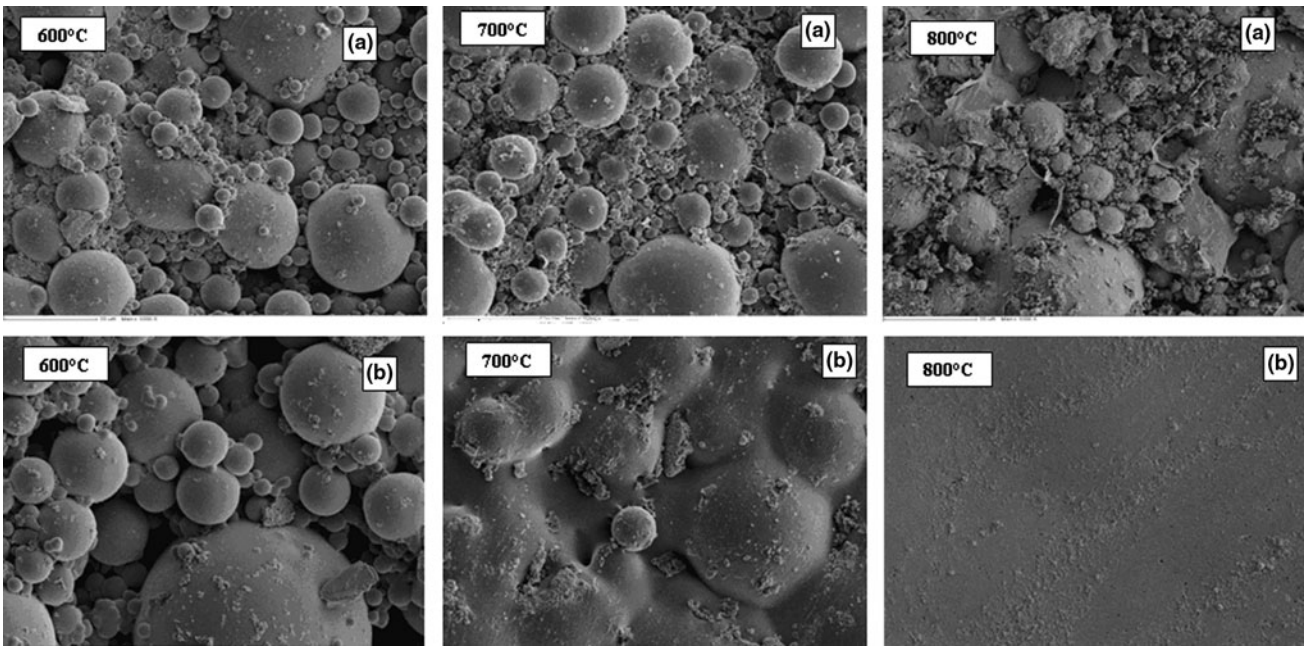

Fig. 21 SEM micrographs of the glass samples sintered in vacuum (**a**), in air (**b**) at different sintering temperatures

parameters. The paper demonstrates that glass injection moulding could be an adequate process to get structured glass parts with well defined geometries, and proper resulting mechanical characteristics.

In a third stage, sintering was conducted at five different sintering temperatures. The experiment results after debinding and sintering stages confirm that the components exhibit anisotrope shrinkage in range from 10 to 20 %. We have also discussed the effects of sintering temperatures on the sintered density, roughness and dimensional stability of injection moulded replicas. The results reveal that high densities can be obtained using sintering above 700 °C, but it affect the dimensional precision as well as roughness surface.

Finally, the parts (after moulding, debinding and air sintering processing steps) obtained PIM exhibit proper shape retention, without visible defects, such as warpage, incomplete filling and crack. The dimensions of the parts

Fig. 22 Photograph of sintered glass components (**a**) vacuum sintered, **b** air sintered

changed with the different processing steps. High densification was achieved at 700 °C.

References

Boccaccini AR, Olevsky EA (1999) Processing of platelet-reinforced glass matrix composites: effect of inclusions on sintering anisotropy. J Mater Process Technol 96:92–101

Cansell F, Aymonier C (2009) Design of functional nanostructured materials using supercritical fluids. J Supercrit Fluids 47:508–516

Czarwinski C (1968) Szklo and Ceram 19:72–75

Gulsoy HO, German RM (2008) Production of micro-porous austenitic stainless steel by powder injection moulding. Scr Mater 58:295–298

Kingeri WD, Berg M (1955) Studies of initial stages of sintering solid by viscous flow, evaporation–condensation and sell-diffusion. J Appl Phys 10:1205–1206

Meng J, Loh NH, Fu G, Tay BY, Tor SB (2011a) Micro powder injection moulding of alumina micro-channel part. J Eur Ceram Soc 31:1049–1056

Meng J, Loh NH, Tay BY, Tor SB, Fu G, Khor KA, Yu L (2011b) Pressureless spark plasma sintering of alumina micro-channel part produced by micro powder injection moulding. Scr Mater 64:237–240

Merz L, Rath S, Piotter V, Ruprecht R, Ritzhaupt-Kleissl J, Hausselt J (2002) Feedstock development for micro powder injection molding. Microsyst Technol 8:129–132

Petzoldt F (2008) Micro powder injection moulding-challenges and opportunities. Powder Inject Mould Int 2:37–42

Pirhonen E, Moimas L, Väänänen P (2006) Porous bioactive glass scaffold with high compression strength. Eur Cells Mater 12:67

Ran T (2001) Compaction and sintering behaviour of glass-alumina composites. Mater Chem Phys 67:220–225

Tay BY, Liu L, Loh NH, Tor SB, Murakoshi Y, Maeda R (2005) Injection moulding of 3D microstructures by μPIM. Microsyst Technol 11:210–213

Wiest A, Harmon JS, Demetriou MD, Conner RD, Johnson WL (2009) Injection molding metallic glass. Scr Mater 60:160–163

Yong-Taeg O, Fujino S, Morinaga K (2002) Fabrication of transparent silica glass by powder sintering. Sci Technol Adv Mater 3:297–301